A least square study on flow and radiative heat transfer of a hybrid nanofluid in a moving frame by considering a spherically-shaped particle

K. Ganesh Kumar[a], M. Gnaneswara Reddy[b], S.A. Shehzad[c,*], and F.M. Abbasi[d]
[a]*Department of Mathematics, SJM Institute of Technology, Chitrdurga-577502, Karnataka, India.*
[b]*Department of Mathematics, Acharya Nagarjuna University Campus, Ongole - 523 001, A.P., India.*
[c]*Department of Mathematics, COMSATS University Islamabad, Sahiwal 57000, Pakistan.*
[*]*e-mail: ali_qau70@yahoo.com*
[d]*Department of Mathematics, COMSATS University Islamabad, Islamabad 44000, Pakistan.*

Received 9 May 2019; accepted 7 September 2019

The focus of this work is to elucidate the nature of a hydrodynamic hybrid nanofluid in a moving frame. Solar radiation and the spherically-shaped particle approximation are implemented. The implication of suitable transformation corresponds to self-similarity equations. Least square and RKF 45^{th}-order techniques are employed to evaluate these non-dimensional equations. For better understanding of the problem, energy and flow features are demonstrated for distinct physical constraints. It is recognized that the transfer of fluid heat is pronounced for enhancing R but dismisses in rising values of Pr. A higher value of indicates that more heat is transferred to the liquid, which translates into a a temperature rise.

Keywords: Solar radiation; spherical shape particle; least square method; hybrid nanofluid.

DOI: https://doi.org/10.31349/RevMexFis.66.162

1. Introduction

The flows over a moving frame have captured the attention due to the various ramifications in multiple processes of engineering.. Having such important implications in view, Bachok *et al*. [1,2] discussed the nanofluids flows in the presence of a moving surface. Turkyilmazoglu [3] executed a time-dependent convection analysis of the flow induced by a vertical surface under heat transportation. Thumma *et al*. [4] studied the natural convective flow of MHD nanofluids over a plate by considering the temperature gradients with suction. The topic of boundary-driven flows on moving surfaces has been elaborated by many; see, for example, [5-9].

At present, nanomaterials have been subject of increasing interest. The concept of hybrid nanofluid is the latest advancement in the theory of nanofluids to improve the rate of heat transportation in engineering, industrial, and technological processes. These hybrid nanofluids have multiple appliances across fields such as acoustics, medicine, transportation, hybrid-powered procedures, micro-fluidics, naval structures, solar accumulators, energy and engine cells, etc. In accordance with such powerful implications, Jana *et al*. [10] investigated the heat transport in hybrid nano-fluidics. Suresh *et al*. [11] analyzed the Cu- Al_2O_3-water hybrid nanofluid under the transportation of heat. Vafaei *et al*. [12] investigated the evolution of thermal conductivity in hybrid nanomaterials. Later on, distinct experimental and theoretical models have been developed to examine the multi-dimensional behavior of hybrid nanofluids [13-17].

Modern efforts have focused on introducing and developing more efficient and affordable technologies for energy storage. For example, nanomaterials are regarded as the best coolants in, among others, aerospace, optics, transport, nuclear, and aircraft industries. In this direction, Rashidi *et al.* [18] reported the magnetic nanomaterials flow by considering radiation and the presence of the buoyancy effect. Makinde [19] addressed the convected flow of nanomaterial induced by a porous plate by accounting the thermal radiation and mass transportation. Hayat *et al*. [20] executed a study of 3D non-Newtonian nanomaterial flow under radiative phenomena. Some featured works in revolution of nanofluid theory can be consulted through [21-30].

Here, our primary motive is to evaluate the aspects of heat transport and flow of a hybrid nanofluid under moving frame by considering spherically-shaped particles. The nonlinear phenomenon of thermal radiation is also taken into account; thus, a more realistic setting is proposed in comparison to the linearized thermal radiation case. According to literature review, no investigation with such physical flow features is reported yet. Elucidations are made with the help of Runge-Kutta-Fehlberg-45 method.

2. Mathematical modeling

Consider a steady-state flow and heat transportation of a hybrid nanofluid in a moving frame. The plate is stretched along the opposite or same direction having free-stream velocity U_∞ and constant velocity U_w. The nonlinear thermal radiation aspects are also taken into account. The flow is confined

to $y > 0$ and the sheet coincides with the plane $y = 0$. The ambient fluid temperature is represented by T_∞.

Governing equations of hybrid nanofluid are defined as:

$$\frac{\partial u}{\partial x} + \frac{\partial v}{\partial y} = 0, \tag{1}$$

$$u\frac{\partial u}{\partial x} + v\frac{\partial v}{\partial y} = \frac{\mu_{hnf}}{\rho_{hnf}}\frac{\partial^2 u}{\partial y^2}, \tag{2}$$

$$(\rho c_p)_{hnf}\left[u\frac{\partial T}{\partial x} + v\frac{\partial T}{\partial y}\right] = \frac{\partial}{\partial y} \times\left[k_{hnf}+\frac{16\sigma^* T^3}{3k^*}\frac{\partial T}{\partial y}\right]+\left(\frac{\partial T}{\partial y}\right)^2, \tag{3}$$

where u and v denote the velocity components of the nanofluid along the x and y directions, respectively, σ^* the Stefan-Boltzmann constant, k^* the mean absorption coefficient and q_r the radiated surface heat flux.

The expressions for viscosity, thermal conductivity, specific heat and density of the hybrid nanofluid are as follows [16]:

$$\begin{aligned}
\mu_{hnf} &= \frac{\mu_f}{(1-\phi_1)^{2.5}(1-\phi_2)^{2.5}},\\
\frac{k_{hnf}}{k_{bf}} &= \frac{k_{s2}+(n-1)k_{bf}-(n-1)\phi_2(k_{bf}-k_{s2})}{k_{s2}+(n-1)k_{bf}+\phi_2(k_{bf}-k_{s2}),}\\
(\rho C_p)_{hnf} &= \Big[(1-\phi_2)[(1-\phi_1)(\rho Cp)_f + \phi_1(\rho Cp)_{s1}] + \phi_2(\rho Cp)_{s2}\Big],\\
\rho_{hnf} &= \Big[(1-\phi^2)\{(1-\phi_1)\rho_f+\phi_1\rho_{s1}\} + \phi_2\rho_{s2}\Big],
\end{aligned} \tag{4, 5}$$

$$\frac{k_{bf}}{k_f} = \frac{-(n-1)\phi_1(k_f-k_{s1}+k_{s1}+(n-1)k_f)}{\phi_1(k_f-k_{s1})+k_{s1}+(n-1)k_f} \tag{6}$$

where $n = 3$ represents the case for spherical nanoparticles. The basic thermo-physical features of nanofluid at 25°C are given in Table I.

TABLE I. Thermo-physical features of Se (nanoparticles), Fe_2O_3 and H_2O (base-fluid).

Property	Se	Fe_2O_3	H_2O
Density (kg m^{-3})	4790	3970	997.1
Thermal conductivity ($WK^{-1}m^{-1}$)	0.519	6	0.6071
Heat capacity (JK^{-1})	3211.27	670	4179

Interrelated boundary conditions are as follows:

$$\begin{aligned}
&u = U_w, \quad v = 0, \quad T = T_w \quad \text{at} \quad y = 0,\\
&u \to U_\infty, \quad T \to T_\infty \quad \text{as} \quad y \to \infty.
\end{aligned} \tag{7}$$

Now, we introduced the similarity transformation as

$$\begin{aligned}
&u = Uf'(\eta), \quad v = \sqrt{\frac{v_f U}{2x}}(\eta f'(\eta) - f(\eta)),\\
&T = T_w(1+(\theta_w-1)\theta(\eta)), \quad \eta = \sqrt{\frac{U}{2v_f x}}y,
\end{aligned} \tag{8}$$

where $U = U_w + U_\infty$, $\theta_w = (T_\infty/T_w)$, $\theta_w > 1$.

Making use of Eq. (8), Eq. (1) is identically satisfied and Eqs. (2) and (3) take the form:

$$\frac{f'''}{\left[(1-\theta_2)\left\{\phi_1\left(\frac{\rho_{s1}}{\rho_f}\right)+(1-\phi_1)\right\}+\phi_2\left(\frac{\rho_{s2}}{\rho_f}\right)\right] * \left[(1-\phi_1)^{2.5}(1-\phi_2)^{2.5}\right]} + ff'' = 0, \tag{9}$$

$$\begin{aligned}
&\frac{k_{nf}}{k_f}R\big[(1+(\theta_w-1)\theta)^3\theta'' + 3(\theta_w-1)\theta'^2(1+(\theta_w-1)\theta)^2\big]\\
&\quad + Pr\left[(1-\theta_2)\left[\phi_1\left(\frac{(\rho Cp)_{s1}}{(\rho Cp)_f}\right)+(1-\phi_1)\right]+\phi_2\left(\frac{(\rho Cp)_{s2}}{(\rho Cp)_f}\right)\right](f\theta' + Ecf''^2) = 0.
\end{aligned} \tag{10}$$

Note that the Eqs. (9) and (10) are transformed form of Eqs. (2) and (3). These expressions are obtained by putting the values of similarity variables given in Eq. (8).

The boundary conditions are converted into the form:

$$f(0) = 0, \quad f'(0) = A, \quad \theta(0) = 1 \quad \text{at} \quad \eta = 0, \quad f'(\infty) = 1 - A, \quad \theta(\infty) = 0, \quad \text{as} \quad \eta \to \infty, \tag{11}$$

where $A = U_w/U_\infty$ the parameter of velocity ratio, $Pr = (\mu Cp)_f/k_f$ the Prandtl number, $Ec = U_w^2/(T_w - T_\infty)C_p f)$ the Eckert number and $R = (16\sigma^* T_\infty^3)/(3k_{hnf}k^*)$ is the radiation parameter. The friction factor (C_{fx}) and local Nusselt number (Nu_x) are prescribed as:

The friction factor (C_{fx}) and local Nusselt number (Nu_x) are prescribed as:

$$C_f = \frac{\tau_w}{\rho_f U_w^2}, \quad Nu_x = \frac{x q_w}{k_f(T_w - T_\infty)} \frac{\partial T}{\partial y}\Big|_{y=0},$$

where τ_w the shear stress and q_w the radiative heat flux and can be expressed as:

$$\tau_w = \mu_{nf}\left(\frac{\partial u}{\partial y}\right),$$

$$q_w = -k_{hnf}\frac{\partial T}{\partial y} + (qr)_w \quad at \quad y = 0.$$

After Utilization of Eq. (8), C_{fx} and Nu_x can be transformed as

$$\sqrt{Re_x}C_{fx} = \frac{1}{(1-\phi)^{2.5}} f''(0),$$

$$\frac{Nu_x}{\sqrt{Re_x}} = -\frac{k_{hnf}}{k_f}(1 + R\theta_w^3)\theta'(0),$$

where $Re = U_x/v_f$ is local Reynolds number.

3. Least square technique

This section elucidates the procedure of least square method. Least square scheme is applied to found the numerical iterations of the problem. This technique is very efficient and straight forward and has the following steps [26]:

Step 1: Equations (9) and (10) can be rewritten as

$$\frac{1}{\left[(1-\phi_2)\left\{\phi_1\left(\frac{\rho_{s1}}{\rho_f}\right) + (1-\phi_1)\right\} + \phi_2\left(\frac{\rho_{s2}}{\rho_f}\right)\right] * \left[(1-\phi_1)^{2.5}(1-\phi_2)^{2.5}\right]} \frac{d^3}{d\eta^3} f(\eta) + f(\eta)\frac{d^2}{d\eta^2} f(\eta) = 0, \tag{12}$$

$$\frac{k_{nf}}{k_f} R\left[\left(1 + (\theta_w - 1)\theta\right)^3 \frac{d^2}{d\eta^2}\theta(\eta) + 3(\theta_w - 1)\left(\frac{d}{d\eta}\theta(\eta)\right)^2 (1 + (\theta_w - 1)\theta(\eta))^2\right]$$

$$+ Pr\left[(1-\theta_2)\left[\phi_1\left(\frac{(\rho Cp)_{s1}}{(\rho Cp)_f}\right) + (1-\phi_1)\right] + \phi_2\left(\frac{(\rho Cp)_{s2}}{(\rho Cp)_f}\right)\right]\left(f(\theta)\frac{d}{d\eta}\theta(\eta) + Ec\frac{d^2}{d\eta^2} f(\eta)\right) = 0. \tag{13}$$

Step 2: To interpret the solutions of the Eqs. (12) and (13), the following trial-based solutions are suggested:

$$\tilde{f}(\eta) = \sum_{K=1}^{N} A_k \eta^k = A_1 + A_2\eta + A_3\eta^2 + \ldots + A_N\eta^N, \tag{14}$$

$$\tilde{\theta}(\eta) = \sum_{K=1}^{N} A_{k+N}\eta^k = A_{N+1} + A_{N+2}\eta + A_{N+3}\eta^2 + \ldots + A_{2N}\eta^N. \tag{15}$$

In the above expressions, N indicates the number of approximations. N is large for more accurate solutions. The ansatz of Eqs. (14) and (15) must satisfy the boundary conditions associated with Eqs. (9) and (10). The solutions can be written as:

$$\tilde{f}(\eta) = \alpha + (1-\phi_1)^{2.5}\eta\eta_\infty - \frac{1}{2}\eta^2(1-\phi)^{2.5}(1-\phi)^{2.5} + \sum_{k=1}^{N} A_k(\eta^{k+1} - (k+2)\eta_\infty^{k+1})\eta, \tag{16}$$

$$\tilde{\theta}(\eta) = 1 - \frac{1}{\eta_\infty}\eta\sum_{K=1}^{N} A_{K+N}(\eta^k - \eta_\infty^k)\eta. \tag{17}$$

Step 3: The residual vectors for each expression in Eqs. (12) and (13) are further developed, by using the reduced trial solution, to obtain

$$R_f = \frac{1}{\left[(1-\phi_2)\left\{\phi_1\left(\frac{\rho_{s1}}{\rho_f}\right) + (1-\phi_1)\right\} + \phi_2\left(\frac{\rho_{s2}}{\rho_f}\right)\right] * \left[(1-\phi_1)^{2.5}(1-\phi_2)^{2.5}\right]} \frac{d^3}{d\eta^3}\tilde{f}(\eta) + \tilde{f}(\eta)\frac{d^2}{d\eta^2}\tilde{f}(\eta) \cong 0,$$

$$R_\theta = \frac{k_{nf}}{k_f} R\left[\left(1 + (\theta_w - 1)\theta\right)^3 \frac{d^2}{d\eta^2}\tilde{\theta}(\eta) + 3(\theta_w - 1)\left(\frac{d}{d\eta}\tilde{\theta}(\eta)\right)^2 (1 + (\theta_w - 1)\tilde{\theta}(\eta))^2\right]$$

$$+ Pr\left[(1-\phi_2)\left[\phi_1\left(\frac{(\rho Cp)_{s1}}{(\rho Cp)_f}\right) + (1-\phi_1)\right] + \phi_2\left(\frac{(\rho Cp)_{s2}}{(\rho Cp)_f}\right)\right]\left(\tilde{f}(\eta)\frac{d}{d\eta}\tilde{\theta}(\eta) + Ec\frac{d^2}{d\eta^2}\tilde{f}(\eta)\right) \cong 0.$$

Step 4: The reduced form of the trial solutions is the exact solutions of Eqs. (14)-(17) by vanishing the residual vectors. The construction of subsequent relations is made fout of the residuals

$$E_f = \int_{\Gamma} R_f^2 d\eta, \quad E_\theta = \int_{\Gamma} R_\theta^2 d\eta. \tag{18}$$

Here the problem domain is represented by Γ. A minimum of Eq. (18) can be achieved by the derivatives of Eq. (18) with respect to the unknowns A_i, which must vanish, so to have

$$\frac{\partial E_f}{\partial A_i} = 2\int R_f(\eta)\frac{\partial R_f}{\partial A_i}d\eta = 0,$$
$$i = N+1, N+2, \ldots, N, \tag{19}$$
$$\frac{\partial E_\theta}{\partial A_i} = 2\int R_\theta(\eta)\frac{\partial R_\theta}{\partial A_i}d\eta = 0,$$
$$i = N+1, N+2, \ldots, 2N, \tag{20}$$

where the factor 2 can be ignored.

Step 5: To obtain the values of all $A_i's$, we solved the system of algebraic expressions obtained from Eqs. (19) and (20). The substitution of the values of the $A_i's$ into the reduced trial solution yields the desired solutions of Eqs. (11)-(14).

4. Results and discussion

The objective of the present study is to extend the work of nanofluids to hybrid nanofluids in the presence of a moving plate by considering nonlinear radiative heat transfer and viscous dissipation. The model equations are transformed with the help of similarity transformations. Further, the obtained similarity equations have been solved numerically. The variations of embedded parameters on friction factor and heat transfer characteristics are shown numerically and graphically.

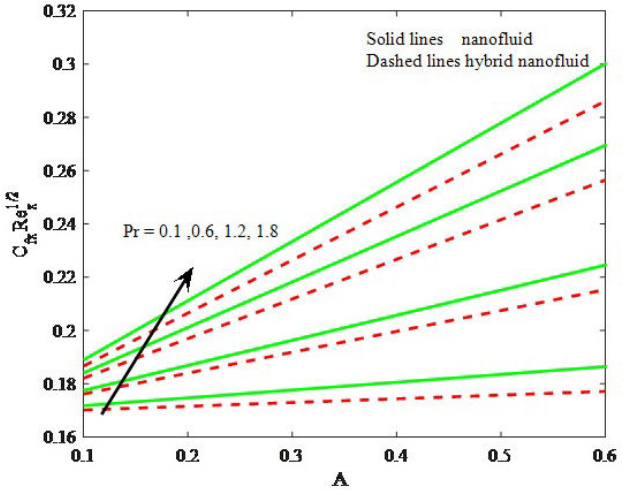

FIGURE 1. Variations of A and Pr on C_{fx}.

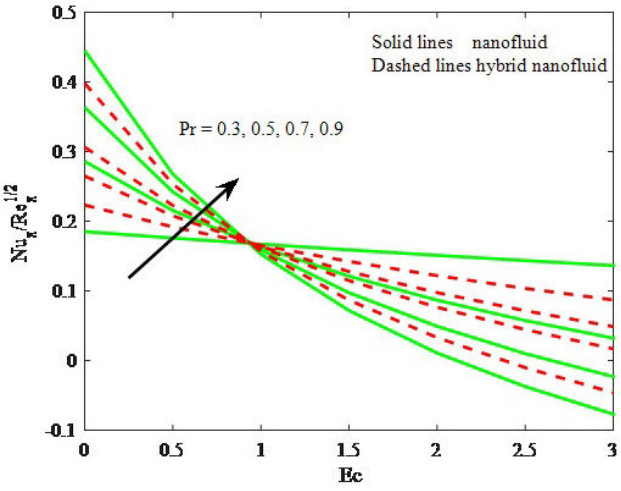

FIGURE 2. Variations of Ec and Pr on Nu_x.

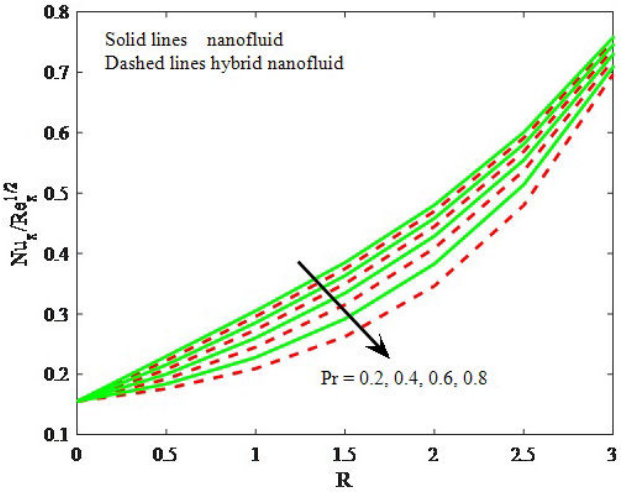

FIGURE 3. Variations of R and Pr on Nu_x.

Fluctuation in skin friction coefficient is presented in Fig. 1 for distinct values of Pr and A for both nanofluid and hybrid nanofluid. Here one can see that an increment in Pr and A leads to an enhancement of the friction factor for both the nanofluid and the hybrid nanofluid. Further, the nanofluid shows overriding performance compared to the hybrid nanofluid The variations in Nu_x through Pr and Ec for both nano and hybrid nanofluids are described in Fig. 2. The higher Pr scale back the Nu_x but in the other hand, Nu_x increases for ascending values of Ec. A comparative analysis shows that the reduction in Nu_x is higher for the hybrid nanofluid case than the nanofluid. The influence of R and Pr on Nu_x is portrayed in Fig. 3. This plot shows that the heat transport rate reduces for higher values of Pr, while a contradiction is recognized for increasing value of R.

The profile of $\theta(\eta)$ versus η is observed in Fig. 4. This figure illustrates that $\theta(\eta)$ is improved rapidly as R is incremented. Physically, a higher value of R corresponds to a higher thickness of the thermal layer. The larger R leads to a decrement in the coefficient of mean absorption.

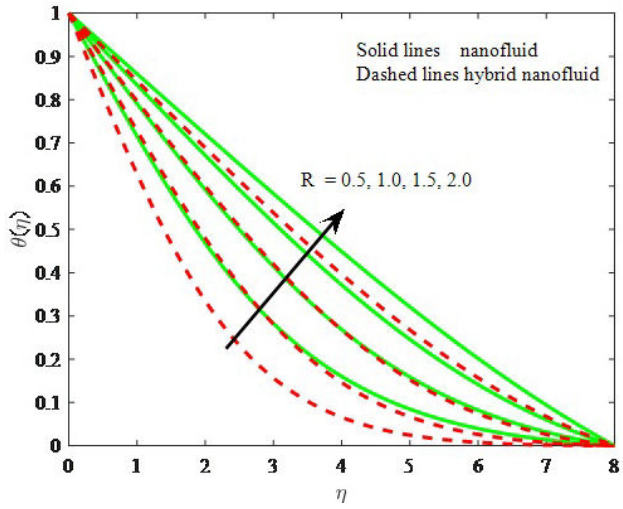

FIGURE 4. Variations of R on $\theta(\eta)$

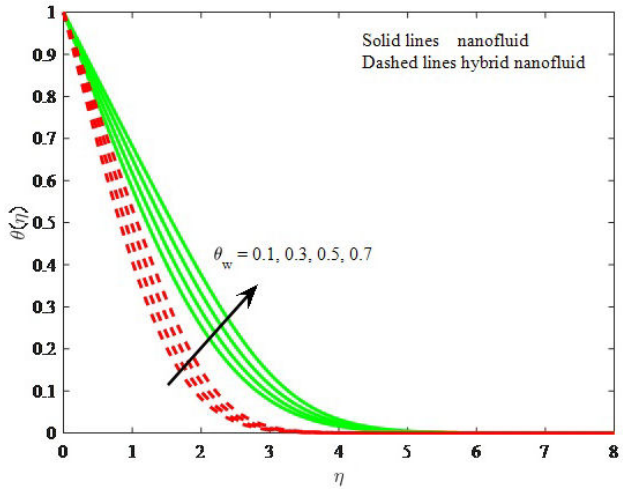

FIGURE 5. Variations of θ_w on $\theta(\eta)$.

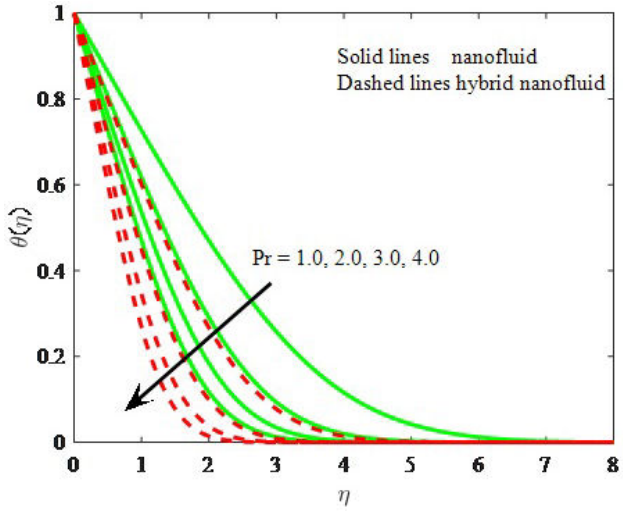

FIGURE 6. Variations of Pr on $\theta(\eta)$.

Hence, the heat amount transfer to liquid is stirring. Fluctuations in $\theta(\eta)$ via θ_w are depicted in Fig. 5. An increase in θ_w corresponds to a higher temperature and thicker thermal layer. The larger θ_w provides more energy to working liquid due to which presence of θ_w give peak to temperature profile. Figure 6 exhibits the role of Pr on the profile of $\theta(\eta)$. A raise in values of Pr diminish the temperature.

Figure 7 presents the influence of Ec on the $\theta(\eta)$ profile. Here, it can be noticed that the temperature and its interrelated thickness of layer is improved for increasing Ec. Basically, the existence of viscous heat in heat expressions acts as an internal heat agent. Hence, the thermal energy booming in the fluid. The effect of ϕ_2 on $f(\eta)$ and $\theta(\eta)$ are demonstrated through Figs. 8 and 9. Figure 8 represents that for larger ϕ_2, the flow is faster for both the nanomaterial and the mixture of nanomaterials. The temperature $\theta(\eta)$ is found to increase for higher ϕ_2 (see Fig. 9). The nanoparticles generate warmness

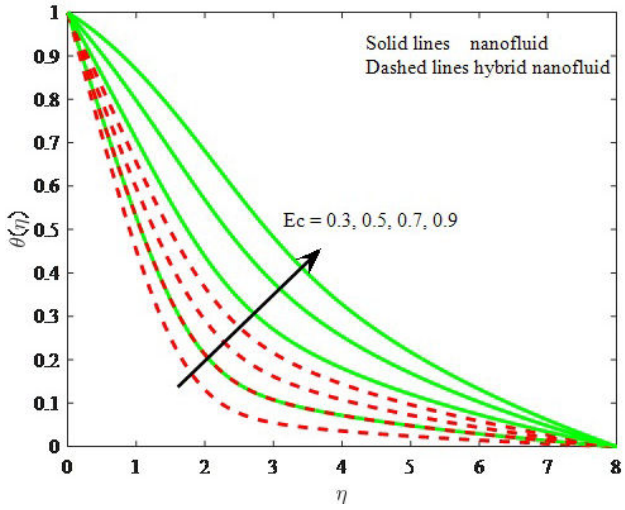

FIGURE 7. Variations of Ec on $\theta(\eta)$.

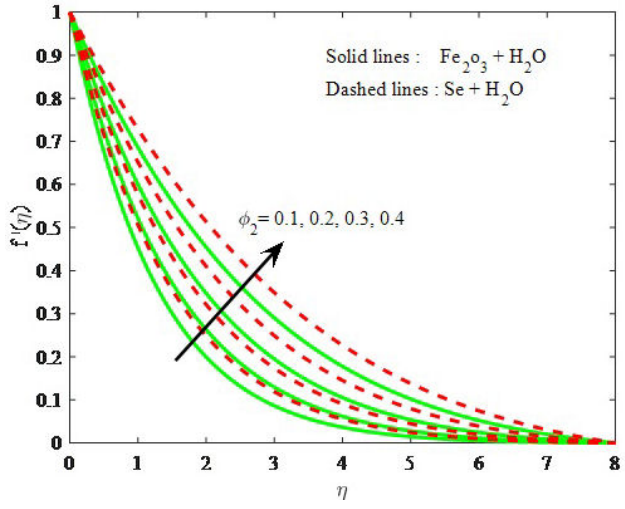

FIGURE 8. Variations of ϕ_2 on $f'(\eta)$.

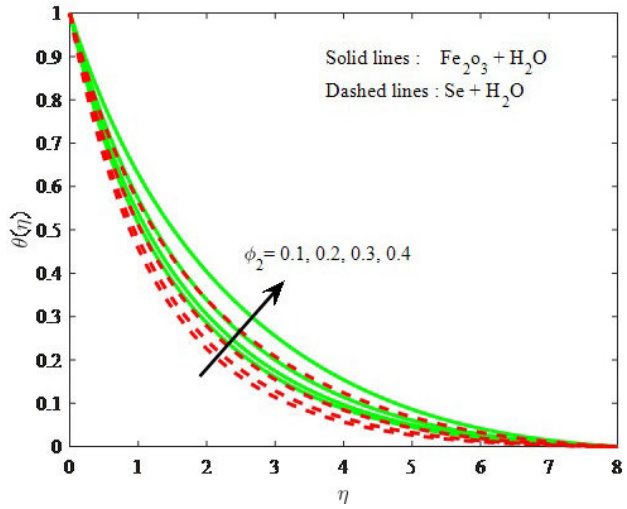

FIGURE 9. Variations of ϕ_2 on $\theta(\eta)$.

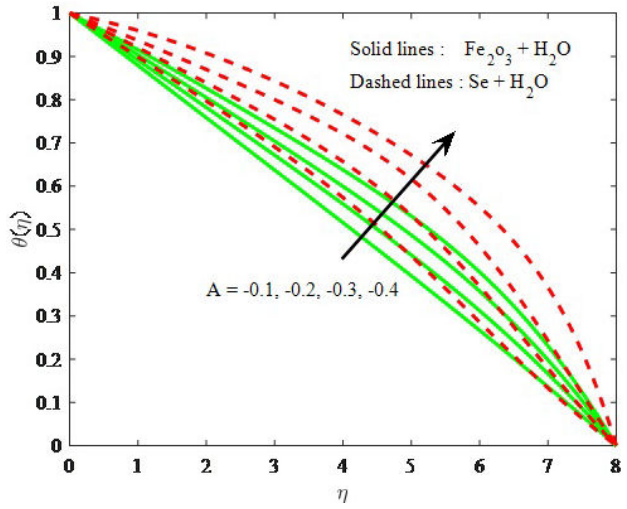

FIGURE 10. Variations of A on $\theta(\eta)$.

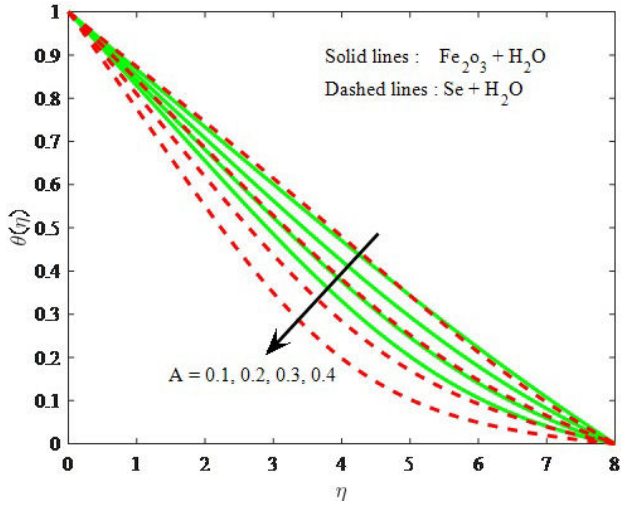

FIGURE 11. Variations of A on $\theta(\eta)$.

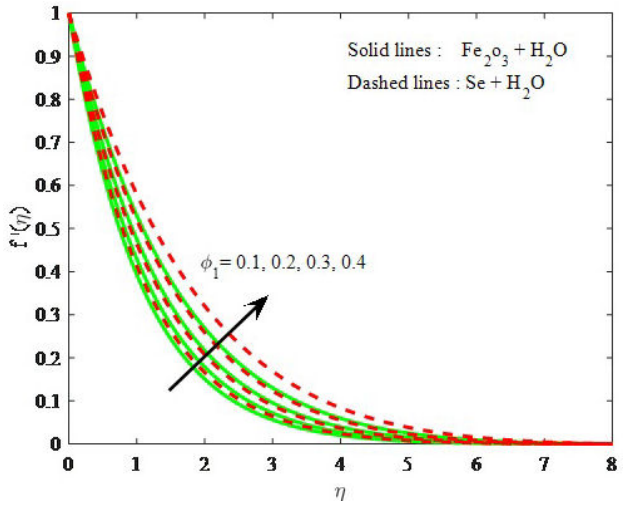

FIGURE 12. Variations of ϕ_1 on $f'(\eta)$.

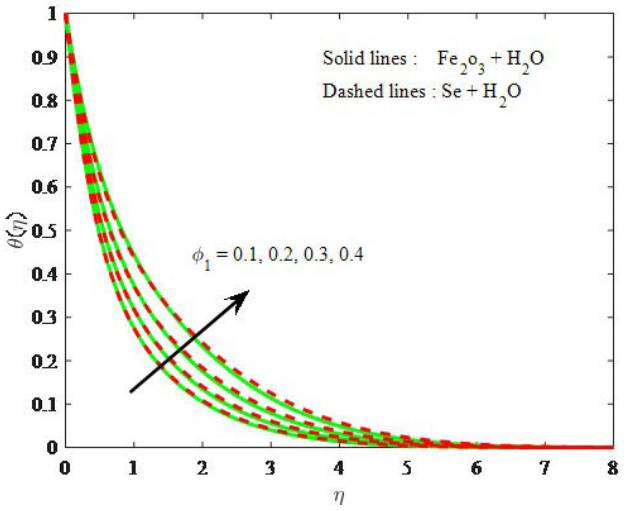

FIGURE 13. Variations of ϕ_1 on $\theta(\eta)$.

in liquid due to presence of photo-catalytic aspect. Hence, the addition of more nanoparticles leads to a temperature enhancement.

The effect of A on $\theta(\eta)$ is portrayed in Figs. 10 and 11. From Fig. 10, it is noticeable that the liquid is close to the surface of the solid on which the liquid flows due to a higher absolute value of $A(< 0)$. Physically, the convection current is improved by an increase in λ. From Fig. 11, one can observe that thetemperature of the fluid scales back for larger values of $A(> 0)$. The behavior of ϕ_1 on both $f'(\eta)$ and $\theta(\eta)$ are plotted in Figs. 12 and 13. From Fig. 12, it is observed that $f'(\eta)$ and its interrelated concentration layer become larger as a function of ϕ_1. Figure 13 indicates that the increasing behavior of $\theta(\eta)$ and its interrelated concentration layer is reduced due to the parameter ϕ_1. Figures 14 and 15 show the stream line graphs for different parameters.

Numeric values of C_{fx} and Nu_x for distinct values of influential constraints are shown in Table II. It was observed that both C_{fx} and Nu_x increase for greater values of A (see Table II).

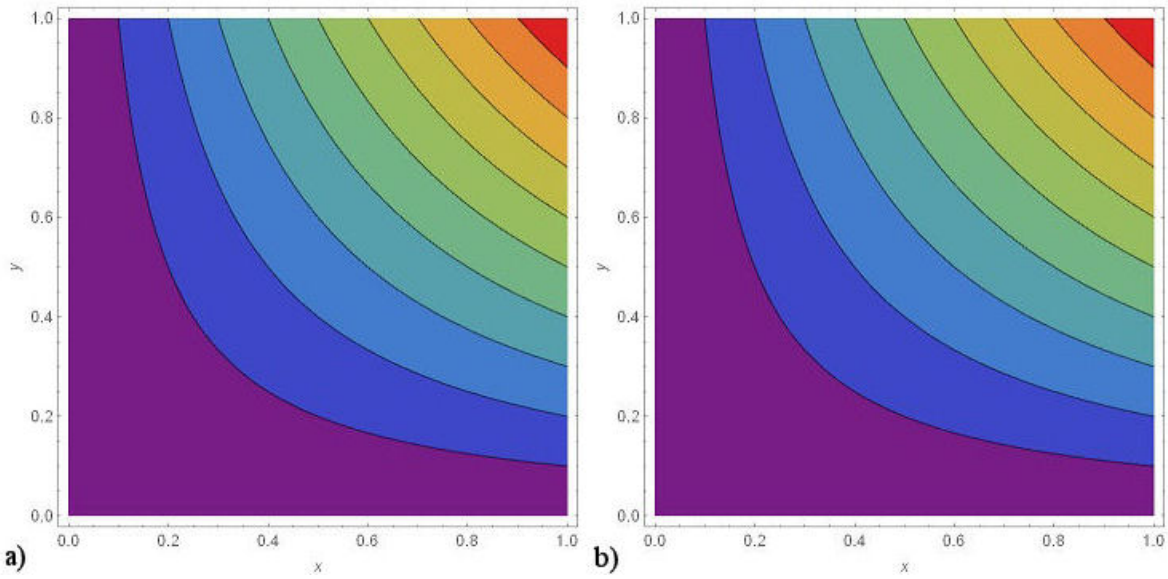

FIGURE 14. a) Stream lines for nanofluid, b) Stream lines for hybrid nanofluid.

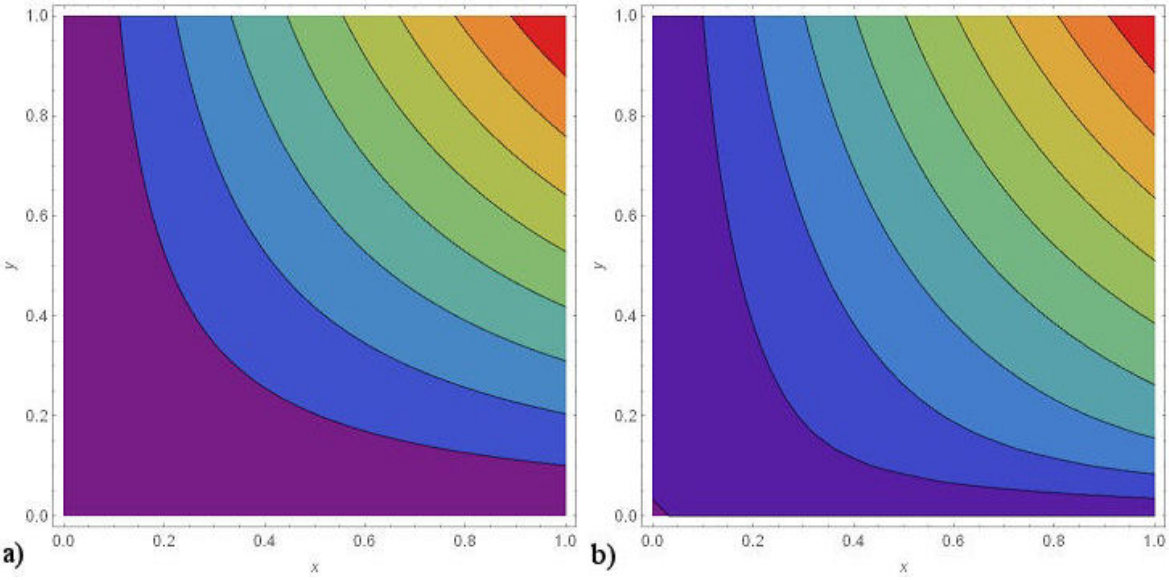

FIGURE 15. a) Stream lines of nanofluid for $A = 1$, b) Stream lines of hybrid nanofluid for $A = 1$.

Moreover Nu_x rises with R and θ_w. Furthermore, from Table II one can see that Nu_x decreases with Ec. It can be noted from Table II that the thermal conductivity of hybrid nanomaterials high in comparison to a regular nanomaterial.

5. Conclusions

The impact of hybrid nanoparticles on fluid flow on a moving plate in the presence of thermal radiation is evaluated. The nonlinear thermal radiation is considered in the energy expression. Further, we visualized that the admixture of distinct nanomaterials corresponds to a high heat capacity in comparison to a regular nanofluid. The most notable outcomes of this study are:

- The addition of hybrid nanomaterials has an positive impact on efficiency in the process of heat transport in comparison to a regular nanoparticles mixture.
- The temperature field is found to decrease rapidly for distinct values of $A < 0$.
- An increase in heat is noted for larger values of R. This translates into a temperature rise for big values of the radiation parameter.

TABLE II. Numeric data of C_f and Nu_x corresponding to distinct values of influential constraints for both nanofluid and hybrid nanofluid.

Pr	Ec	θ_w	R	A	$-C_{fx}$		NU_x	
					Hybrid nanofluid	Nanofluid	Hybrid nanofluid	Nanofluid
0.1					0.466102	0.463552	0.177526	0.176076
0.3					0.462809	0.461259	0.191266	0.192070
0.5					0.368881	0.368685	0.191602	0.208061
	0.1				0.478132	0.469114	0.252315	0.191266
	0.3				0.467101	0.465370	0.228968	0.186031
	0.5				0.464508	0.463552	0.208061	0.181655
		0.1			0.463940	0.462285	0.183255	0.180411
		0.2			0.464503	0.462397	0.186977	0.181097
		0.3			0.464974	0.462963	0.191973	0.182820
			0.1		0.466745	0.465113	0.158576	0.177080
			0.2		0.465981	0.464644	0.162353	0.179877
			0.3		0.465214	0.464132	0.166506	0.183226
				0.1	0.087640	0.089699	0.170182	0.186840
				0.2	0.061450	0.078860	0.171862	0.187095
				0.3	0.193750	0.209747	0.173408	0.193058

- A high Prandtl number Pr corresponds to a lower $\theta(\eta)$ profile. This is due to the low thermal diffusivity caused by Pr.
- Temperature $\theta(\eta)$ increases for larger values of ϕ_1.
- An increment in ϕ_2 resulted in an improvement in both $f'(\eta)$ and $\theta(\eta)$ profiles.

Nomenclature

A	velocity ratio parameter
Ec	Eckert number
$T(k)$	temperature of nanofluid
T_∞	temperature of ambient fluid
ρ_{nf}(Kg m^{-3})	Nanofluid effective density
μ_{nf}(Ns m^{-2})	Nanofluid effective viscosity
α_{nf}(m^2 s^{-1})	Nanofluid thermal diffusivity
ρ_{hnf}(Kg m^{-3})	effective density of the hybrid nanofluid
μ_{hnf}(Ns m^{-2})	effective viscosity of hybrid nanofluid
k_{nf}(W K^{-1}m^{-1})	effective thermal conductivity of nanofluid
ϕ_1	solid volume-fraction of aluminium nanoparticle
ϕ_2	solid volume-fraction of copper nanoparticle
ρ_f(Kg m^{-3})	reference density of fluid fraction
ρ_s(Kg m^{-3})	solid-fraction reference density
ρ_{s1}(Kg m^{-3})	solid-fraction reference density
ρ_{s2}(Kg m^{-3})	solid-fraction reference density
K_f (W K^{-1}m^{-1})	fluid thermal conductivity
K_s (W K^{-1}m^{-1})	solid thermal conductivity
K_{s1} (W K^{-1}m^{-1})	solid alumina thermal conductivity
K_{s2} (W K^{-1}m^{-1})	solid copper thermal conductivity
C_s (J K^{-1})	heat capacity of solid surface
Pr	Prandtl number
R	radiation parameter
Re_x	Reynolds Number

Acknowledgments

The authors are thankful to the editor and reviewer for their constructive comments and suggestions to improve the quality of the manuscript.

1. N. Bachok, A. Ishak, and I. Pop, *Int. J. Therm. Sci.* **49** (2010) 1663-1668.
2. N. Bachok, A. Ishak, and I. Pop, *Int. J. Heat and Mass Tran.* **55** (2012) 642-648.
3. M. Turkyilmazoglu, *J. Heat Transger-T. ASME* **136** (2013) 031704-7.
4. S.M. Hussain, J. Jain, G.S. Seth, and M.M. Rashidi, *J. Magn. Magn. Mater.* **422** (2017) 112-123.
5. J. Ma, Y. Sun, and B. Li, *Int. J. Heat Mass Tran.* **114** (2017) 469-482.
6. P.K. Kadiyala, and H. Chattopadhyay, *Heat Transfer Engineering* **39** (2018) 98-106.
7. T. Gul *et al.*, *Appl. Sci.* **7** (2017) 369.
8. K.G. Kumar, B.J. Gireesha, B. C. Prasannakumara, and O. D. Makinde, *Diffusion Foundations* **11** (2017) 22-32.
9. K. G. Kumar, B .J. Gireesha, M. R. Krishnamurthy, and B. C. Prasannakumara, *J. Nanofluids* **7** (2018) 108-114.
10. S. Jana, A. S. Khojin, and W. H. Zhong, *Thermochim. Acta* **462** (2007) 45-55.
11. S. Suresh, K. P. Venkitaraj, P. Selvakumar, and M. Chandrasekar, *Exp. Therm. Fluid Sci.* **38** (2012) 54-60.
12. M. Vafaei *et al.*, *Physica E* **85** (2017) 90-96.
13. M. Hassan, M. Marin, R. Ellahi, and S.Z. Alamri, *Heat Transf. Res.* **49** (2018) 18.
14. G.M. Moldoveanu, G. Huminic, A.A. Minea, and A. Huminic, *Int. J. of Heat Mass Tran.* **127** (2018) 450-457.
15. A. Akhgar, and D. Toghraie, *Powder Technol.* **338** (2018) 806-818.
16. B. Souayeh *et al.*, *J. Mol. Liq.* **290** (2019) 111223.
17. K. G. Kumar, B.S . Avinash, M. Rahimi-Gorji, and I. Alarifi, *J. Mol. Liq.* **293** (2019) 111556.
18. M. M. Rashidi, N. V. Ganesh, A. K. A. Hakeem, and B. Ganga, *J. Mol. Liq.* **198** (2014) 234-238.
19. O. D. Makinde, *Int. Commun. Heat Mass Tran.* **32** (2005) 1411-1419.
20. T. Hayat, M. B. Ashraf, H. H. Alsulami, and M. S. Alhuthali, *Plos One* **9** (2014) e90038.
21. M.G. Reddy, *J. Sci. Res.* **6** (2014) 257-272.
22. J. Li, L. Liu, L. Zheng, and B. Bin-Mohsin, *J. Taiwan Inst. Chem.l E.* **67** (2016) 226-234.
23. K. Hsiao, *Int. J. Heat Mass Tran.* **112** (2017) 983-990.
24. N. Muhammad, S. Nadeem, and R. Haq, *Results Phys.* **7** (2017) 854-861.
25. R. Mehmood, S. Rana, and E. N. Maraj, *Commun. Theor. Phys.* **70** (2018) 70106.
26. M. Sheikholeslami, S.A. Shehzad, and R. Kumar, *Commun. Theor. Phys.* **69** (2018) 667-675.
27. Z. Li, M. Sheikholeslami, M. Jafaryar, A. Shafee, and A.J. Chamkha, *J. Mol. Liq.* **266** (2018) 797-805.
28. T. Liu, L. Liu, and L. Zheng, *Therm. Sci.* **22** (2018) 2803-2813.
29. S. A. Shehzad, *Rev. Mex. Fis.* **64** (2018) 628-633.
30. F. M. Abbasi, I. Shanakhat, and S. A. Shehzad, *Phys. Scripta* **94** (2019) 025001.
31. M. Sheikholeslami *et al.*, *Rev. Mex. Fis.* **65** (2019) 365-372.
32. K. G. Kumar, S. A. Shehzad, T. Ambreen, and M. I. Anwar, *Rev. Mex. Fis.* **65** (2019) 373-381.